Contrast-Enhanced iNAV MRA for Whole-Chest, Whole-Heart, and Whole-Aortic Imaging: A Single-Center Experience

Jason Craft[1], Timothy Carter[2], Joshua Y. Cheng[1], Christopher J. Moran[3], Karl P. Kunze[4], Michaela Schmidt[5], Rene M. Botnar[6,7,8], Claudia Prieto[6,7]

[1]DeMatteis Cardiovascular Institute, St. Francis Hospital & Heart Center, Roslyn, NY, USA
[2]Department of Cardiothoracic Surgery, Good Samaritan University Hospital, West Islip, NY, USA
[3]Department of Radiology, Good Samaritan University Hospital, West Islip, NY, USA
[4]MR Research Collaborations, Siemens Healthcare Limited, Camberley, United Kingdom
[5]Research & Clinical Translation, Magnetic Resonance, Siemens Healthineers, Erlangen, Germany
[6]School of Biomedical Engineering and Imaging Sciences, King's College London, London, United Kingdom
[7]School of Engineering, Pontificia Universidad Católica de Chile, Santiago, Chile
[8]Institute for Biological and Medical Engineering, Pontificia Universidad Católica de Chile, Santiago, Chile

Introduction

Undersampled 3D whole-heart inversion recovery (IR) Dixon gradient echo (GRE) accelerated by variable-density spiral-like Cartesian trajectory (VD-CASPR) with image-based navigators (iNAVs) for motion estimation and nonrigid motion-corrected iterative sensitivity-encoding (SENSE) reconstruction with 100% respiratory scan efficiency has the potential for integration into workflows for left atrial and left ventricular delayed enhancement [1]. Our initial aim was to develop an iNAV-compatible method to provide complementary contrast-enhanced (CE) pulmonary vein magnetic resonance angiography (MRA) for registration with delayed enhancement and high-quality left atrial segmentation, while being insensitive to flow and off-resonance artifacts. The need was compounded by the shortage of iohexol and iodixanol intravenous contrast media products for computed tomography angiography (CTA) from May to June 2022. Single-contrast saturation-recovery (SR) and IR GRE have been widely used for this purpose with excellent results [2, 3], although experience is relegated to diaphragmatic navigator prospective motion correction. Widespread clinical adoption has been constrained by commonly recognized limitations to this approach, including an unpredictable scan duration, and residual respiratory motion due to the inaccurately assumed slab tracking ratio. As a solution, we collaborated with our partners at Siemens Healthineers, at Pontificia Universidad Católica de Chile, and at King's College London to configure both SR and IR GRE for iNAV pulmonary vein CE-MRA, later adapting the IR GRE method for whole-chest angiography (iNAV CE-MRA) [4].

For the majority of patients, 3D non-contrast-enhanced T2-prepared balanced steady-state free precession (bSSFP) provides highly diagnostic image quality. However, iNAV CE-MRA has several key advantages that warrant consideration for use. These include a lack of dependency on chemically selective fat saturation preparatory pulses, which may inadvertently saturate the water signal in the aortic arch and proximal descending aorta [5]; and demonstrably superior blood pool signal uniformity, allowing performance consistency of threshold-based anatomical segmentation used to generate centerline semi-automated aortic measurements (CSAMs). iNAV CE-MRA can also be combined with time-resolved angiography with interleaved stochastic trajectories (TWIST) for comprehensive dynamic 4D angiography. Given the rapidly shifting landscape of modern MR imaging, referral patterns, provider needs, and the increase in patient complexity, it is also increasingly important to have techniques that are robust to susceptibility artifacts from sources such as internal cardiac defibrillators (ICDs)/pacemakers[1], thoracic endovascular aortic repairs (TEVAR)[1], and hybrid aortic repairs. That being said, the technical downside to iNAV CE-MRA is variation in image

[1]*The MRI restrictions (if any) of the metal implant must be considered prior to patient undergoing MRI exam. MR imaging of patients with metallic implants brings specific risks. However, certain implants are approved by the governing regulatory bodies to be MR conditionally safe. For such implants, the previously mentioned warning may not be applicable. Please contact the implant manufacturer for the specific conditional information. The conditions for MR safety are the responsibility of the implant manufacturer, not of Siemens Healthineers.*

contrast with irregular rhythms (which can degrade image quality), more elaborate MRA planning, and risk of MR acquisition mistiming in relation to the delivery of gadolinium-based contrast agent (GBCA). To partially alleviate these shortcomings, the artificial intelligence cardiac scan companion (AICSC)[2] WIP and auto resting-phase detection [6] are promising tools to reduce efficiency overhead, and can be used for automated whole-chest slab placement, navigator placement, and alignment of the data window duration. We also favor the use of a simplified injection scheme that is practical for everyday clinical use without contrast dilution, manipulation of extra tubing, syringes, and/or stopcocks. Lastly, it is feasible to monitor GBCA arrival using the low-resolution 2D iNAV images to minimize the possibility of sequence mistiming error.

Protocols

Exams are performed on a MAGNETOM Sola or MAGNETOM Aera 1.5-Tesla scanner (Siemens Healthineers, Erlangen, Germany) with a dedicated 32-channel spine coil and an 18-channel phased array torso coil. In order to minimize confusion and simplify communication across multiple sites where remote scanning is used, a minimal number of core protocols were developed for use regardless of patient complexity.

To date, we have performed over 300 iNAV CE-MRA exams, over 250 of which were whole-chest or whole-aorta imaging. We have three core protocols for whole-chest and whole-aorta MRA imaging:

1) TWIST followed by iNAV CE-MRA: Appropriate for patients with aortic disease limited to the thoracic aorta.
2) First-pass abdominopelvic MRA followed by iNAV CE-MRA: Used in patients with extensive thoracic and abdominal aortic dissection and surgical repair.
3) TWIST followed by iNAV CE-MRA, then first-pass abdominopelvic MRA: Appropriate for patients with extensive thoracic and abdominal aortic dissection, but with TEVAR or hybrid repairs.

Sequence parameters for TWIST and iNAV CE-MRA can be found in Table 1. Before administering GBCA, we test the fidelity of the vectorcardiogram (VCG) gaiting and perform prescan adjustments to be copied to subsequent iNAV scans by running a copy of the sequence for several seconds.

Separate from the test scan, we create identical pairs of iNAV CE-MRA program steps to be run roughly 10 seconds after TWIST completes, which is enough time to give the patient instructions. As our experience matured, we found it was no longer necessary to insert an injector pause between the bolus and continuous GBCA infusion.

[2]Work in progress. The application is currently under development and is not for sale in the U.S. and in other countries. Its future availability cannot be ensured.

MRA sequence	TWIST	iNAV CE-MRA	iNAV CE-MRA$_{Isotropic}$
FOV (coronal)	400 × 300 × 160 mm	380 × 380 × 157 mm	360 × 360 × 153 mm
In-plane spatial resolution	1.13 × 1.62 mm	1.31 × 1.31 mm	1.25 × 1.25 mm
Phase oversampling	50%	30%	30%
Slice thickness	2 mm	1.4–1.5 mm	1.2 mm
Slice resolution	54%	90%	100%
Acceleration factor	GRAPPA 3	3.2*	4.1*
Sampling distribution	Elliptical scanning 15% (region A), 20% (region B)	Elliptical scanning	Elliptical scanning
Bandwidth	676 Hz/px	755 Hx/px	755 Hx/px
Flip angle	23°	18°	18°
Inversion time	N/A	200–290 ms	200–290 ms
TE/TR	.9 ms/2.4 ms	1.1 ms/3.34 ms	1.17 ms/3.44 ms
Data window duration	N/A	130 ms**	130 ms**

Table 1: Imaging parameters for whole-chest TWIST and iNAV CE-MRA.
*Acceleration factor is increased as needed to fit an acquisition duration of ≤ 5 minutes.
**Data window duration is adjusted as needed according to the optimal cardiac rest period.

The first program step is run to completion if continuous infusion peaking is already evident on the low-resolution inline-display 2D images (this makes the second program step unnecessary). Otherwise, the second program step is run to completion and will need to be triggered at the peak of the continuous infusion via the stop-and-continue function on the inline display (Fig. 1).

iNAV CE-MRA can also be acquired without TWIST for single-station whole-chest angiography. It is the experience of others and our own intuition that 0.075 mmol/kg bolus of a 1-molar agent at 1 mL/s, followed by 0.075 mmol/kg at 0.10 mL/s, and 20–30 mL/saline at 0.10 mL/s provides excellent results [3]. In this case, the first program step is used only for testing the VCG gating fidelity, making pre-scan adjustments, and monitoring the passage of contrast with the image navigator. The second program step, which will run to completion, is triggered at the peak of the continuous infusion.

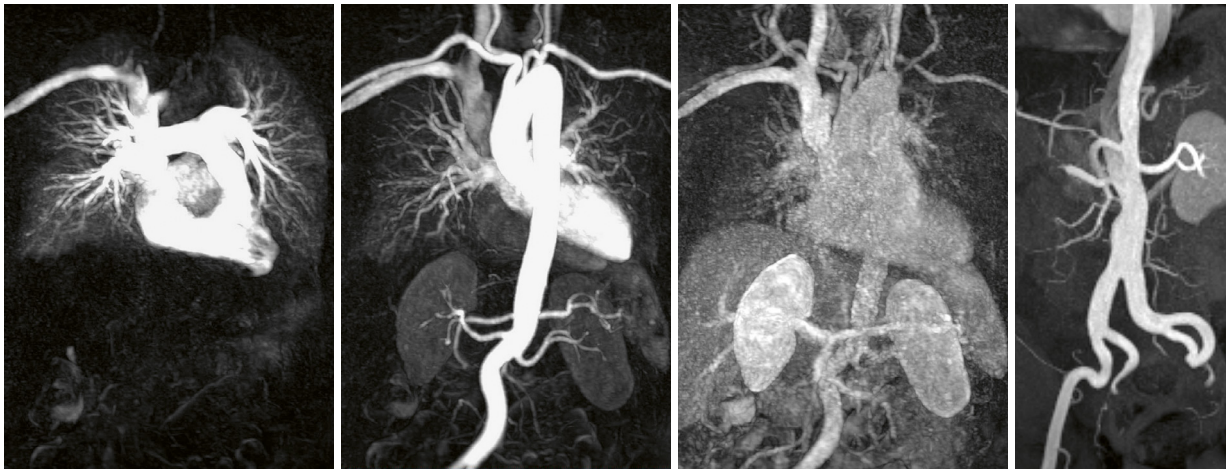

1 **Option 1:** TWIST MRA: 0.05 mmol/kg at 2 ml/s of 1 molar GBCA followed by 30 ml saline **or** **Option 2:** First pass MRA abdomen and pelvis: 0.1 mmol/kg at 2 ml/s of 1 molar GBCA followed by 20–30 ml saline

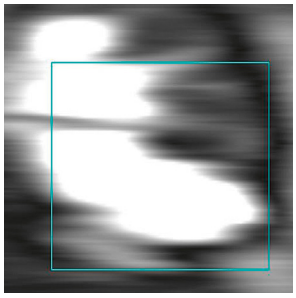

2 Continuous infusion: 0.16 ml/sec GBCA, 20–30 ml saline

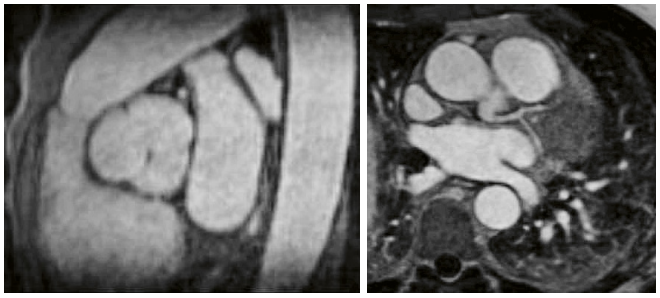

3 iNAV CE-MRA

1 molar GBCA dose: 0.1 mmol/kg

1 Method for whole-chest image-based navigator contrast-enhanced magnetic resonance angiography (iNAV CE-MRA). Two identical 3D whole-chest program steps are created in the workflow. **(1)** Following TWIST (Option 1) or first-pass CE-MRA (Option 2), a continuous infusion of gadolinium-based contrast agent (GBCA) begins **(2)**. The first iNAV program step **(3)** commences afterwards and is run to completion only if the continuous infusion arrival is evident on 2D low-resolution images. Otherwise, the required second program step is triggered as the continuous infusion peaks. If TWIST was performed initially (Option 1), first-pass abdominopelvic MRA can be added after iNAV CE-MRA using 0.05 mmol/kg of 1-molar GBCA.

Use of iNAV CE-MRA in challenging patients

Obesity

From 1990 to 2022, obesity rates more than doubled among women and nearly tripled in men. It is estimated that over 1 billion people worldwide are obese, including 159 million children [7].

In the United States alone, obesity-related healthcare expenditures are estimated to be more than $385 billion in 2024 [8].

High-quality MR imaging in this population poses challenges, such as decreased signal-to-noise ratio (SNR) from reduced radiofrequency penetration, larger acquired voxel dimensions, and increased patient-specific field inhomogeneity as magnetic bore sizes are pushed to the limit. The latter directly contributes to phase incoherency artifacts from T2 and fat saturation preparatory pulses, with large-volume shimming having reduced effectiveness across the whole-chest 3D field of view.

Other modalities are also negatively impacted: Echocardiography with poor acoustic windows and inadequate ultrasound penetration depth, and CT with increased beam attenuation resulting in photon starvation and low SNR.

Although GRE generally has an overall lower SNR in several applications, Tandon et al. demonstrated higher intravascular SNR for gadofosveset-enhanced IR GRE compared to 3D T2-prepared bSSFP [9]. It is yet to be determined if this observation translates to weak albumin-binding GBCAs.

In a single-center study consisting of 65 patients with atrial fibrillation referred for CMRI, mean BMI was 30 ± 6 kg/m^2. However, good or excellent quality pulmonary-vein iNAV CE-MRA was obtained in 95% of exams. Additionally, good or excellent left atrial segmentation was seen in 97% of exams [10].

This helps support the use of MRA in a population that is vulnerable to higher effective radiation doses needed for routine medical imaging [11].

High-quality whole-chest iNAV CE-MRA may also be realized in this patient population. Figure 2 demonstrates two examples where iNAV CE-MRA produced high-quality imaging despite body habitus.

Endografts and implantable cardiac devices[1]

TEVAR is considered first-line therapy for the treatment of complicated Type B aortic dissection (TBAD) and descending thoracic aortic aneurysms [12]. Although the metallic frame structure is readily visible on CT imaging, time-resolved MRA has higher sensitivity for the detection of endoleaks [13]. It is common to encounter intravascular dephasing within the TEVAR using iNAV CE-MRA, but not with TWIST. This signal loss is related to metallic artifact, non-laminar flow, and thus intravoxel velocity heterogeneity. Therefore, TWIST and iNAV CE-MRA are combined for arterial, venous, and delayed phase imaging (Figs. 3, 4). While a TEVAR nitinol exoskeleton composition produces relatively small susceptibility artifacts, the opposite is true regarding ICDs and pacemakers.

Over 200,000 ICDs and 1 million cardiac pacemakers are implanted every year worldwide [14]. Approximately 200,000 cardiac pacemakers are implanted in the United States alone [15], posing a challenge to conventional CMR imaging.

MRA imaging in device patients has historically been an underexplored topic of interest, possibly due to many existing systems containing non-MR-conditional generators or leads. As a consequence, this population may be exposed to recurring doses of ionized radiation (i.e., for annual aortic surveillance).

For these patients, a modified wideband IR pulse with a spectral bandwidth of 2–6 kHz has shown benefit for 3D delayed enhancement, and may have a role in whole-chest angiography [16]. An IR frequency offset may be helpful in shifting artifacts away from pertinent anatomical structures, at the cost of IR efficiency and loss of image contrast. Examples of iNAV CE-MRA with and without wideband IR are found in figures 5, 6, and 7. In contrast, TWIST is more robust due to lack of IR pulse and shorter repetition time, and can provide diagnostic information in areas affected by artifacts on iNAV CE-MRA.

[1] *The MRI restrictions (if any) of the metal implant must be considered prior to patient undergoing MRI exam. MR imaging of patients with metallic implants brings specific risks. However, certain implants are approved by the governing regulatory bodies to be MR conditionally safe. For such implants, the previously mentioned warning may not be applicable. Please contact the implant manufacturer for the specific conditional information. The conditions for MR safety are the responsibility of the implant manufacturer, not of Siemens Healthineers.*

2 Whole-chest iNAV CE-MRA in patients with obesity. **(2A)** Patient 1 with Sievers Type 1 bicuspid aortic valve and thoracic ascending aortic aneurysm, BMI 51 kg/m². **(2B)** CTA images for comparison. **(2C)** Patient 2, status post-thoracic endovascular aortic repair (TEVAR), BMI of 45 kg/m².

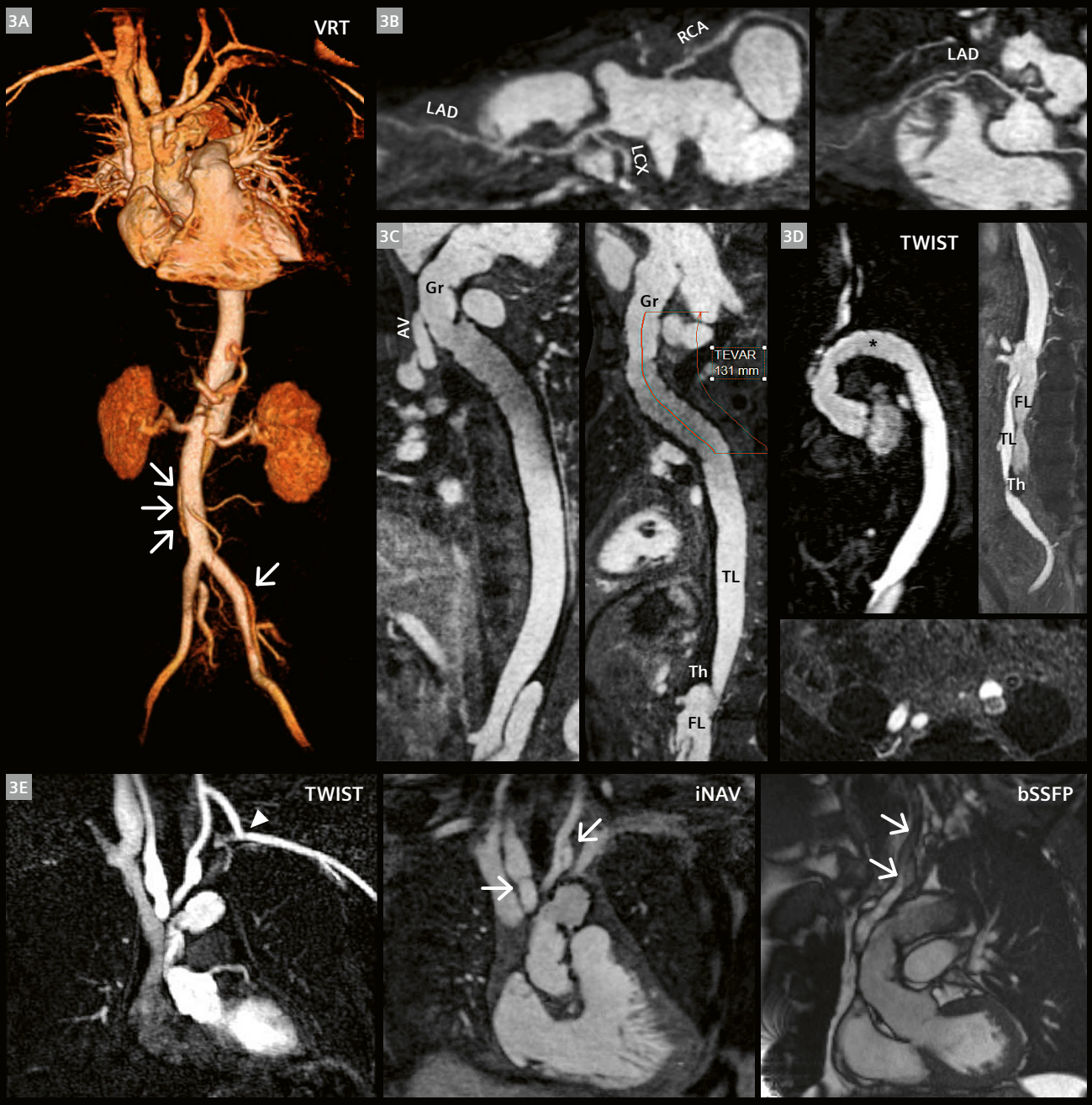

3 A 57-year-old male, Type A aortic dissection, status post-hybrid repair with debranching of the supra-aortic vessels, left common carotid to left subclavian bypass. **(3A)** Composite volume rendering (VRT) of the iNAV and first-pass CE-MRA. **(3B)** The left anterior descending (LAD) artery, right coronary artery (RCA), and left circumflex coronary artery (LCX) are free from dissection. **(3C)** An interposition graft (Gr) is present in the ascending aorta with composite reconstructed arch vessel (AV). The thoracic endovascular aortic repair (TEVAR) graft spanning 131 mm is present in the thoracic descending aorta. Loss of intravascular signal intensity is appreciated within the TEVAR graft. Residual aortic dissection is present in the abdominal aorta, where the true lumen (TL) and false lumen (FL) containing thrombus (Th) can be identified. **(3D)** Compared to iNAV CE-MRA, there is no appreciable signal loss within the TEVAR graft (black asterisk) on arterial phase TWIST. First-pass abdominopelvic CE-MRA redemonstrates the true lumen, false lumen, thrombus, and dissection extension to the level of the common iliac artery. **(3E)** TWIST demonstrates patent left common carotid to left subclavian bypass (white arrowhead). iNAV CE-MRA depicts residual dissection in the brachiocephalic and left common carotid arteries (white arrows). In contrast, balanced steady-state free precession (bSSFP) images are affected by dephasing artifacts in the supra-aortic vessels.

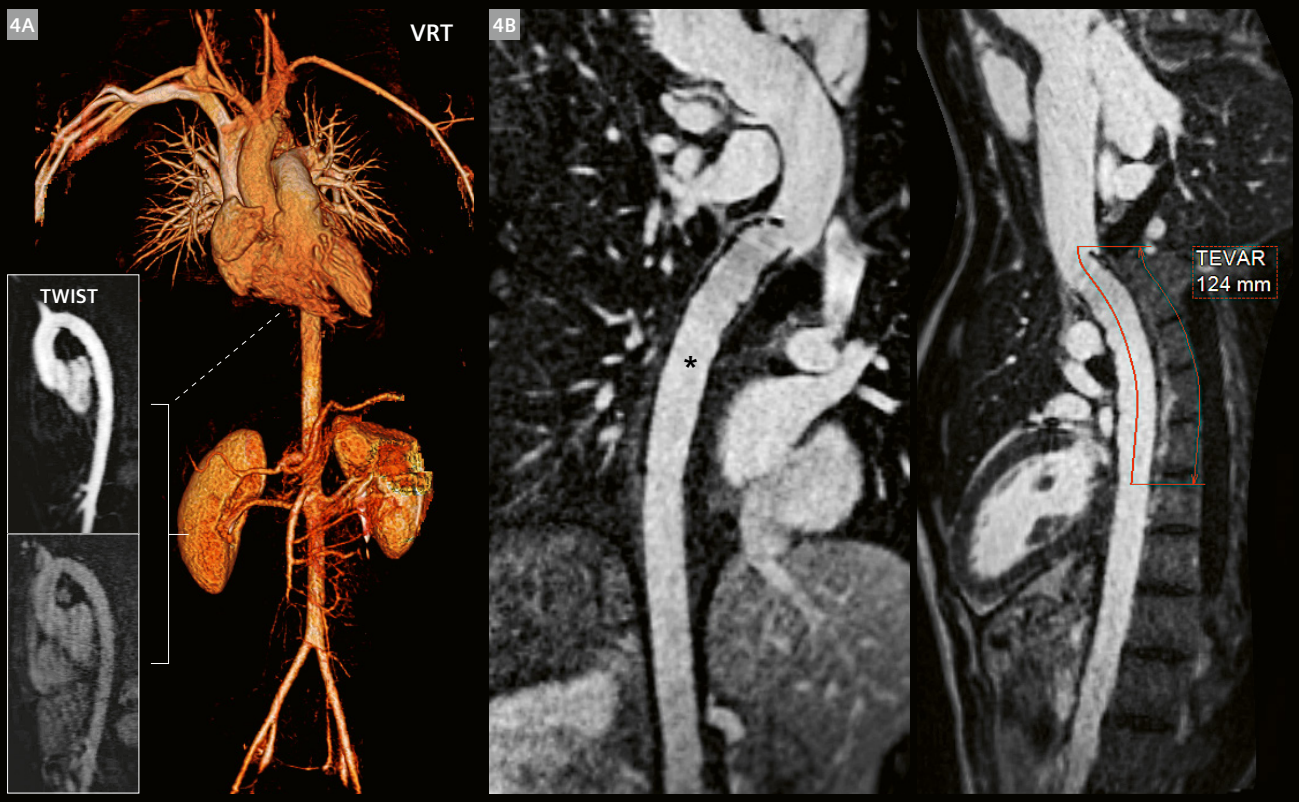

4 iNAV CE-MRA in a patient status post-thoracic endovascular aortic repair (TEVAR). **(4A)** Composite volume rendering (VRT) of iNAV and first-pass abdominopelvic CE-MRA. The inset images demonstrate arterial and venous TWIST phases. There is no evidence of endoleak. **(4B)** Curved multiplanar reconstructions (MPRs) demonstrate the TEVAR graft spanning 124 mm. Minor signal intensity loss is present within the graft (asterisk). **(4C)** Coronal and sagittal maximal intensity projections (MIPs) of the abdominal aorta, which is free from pathology.

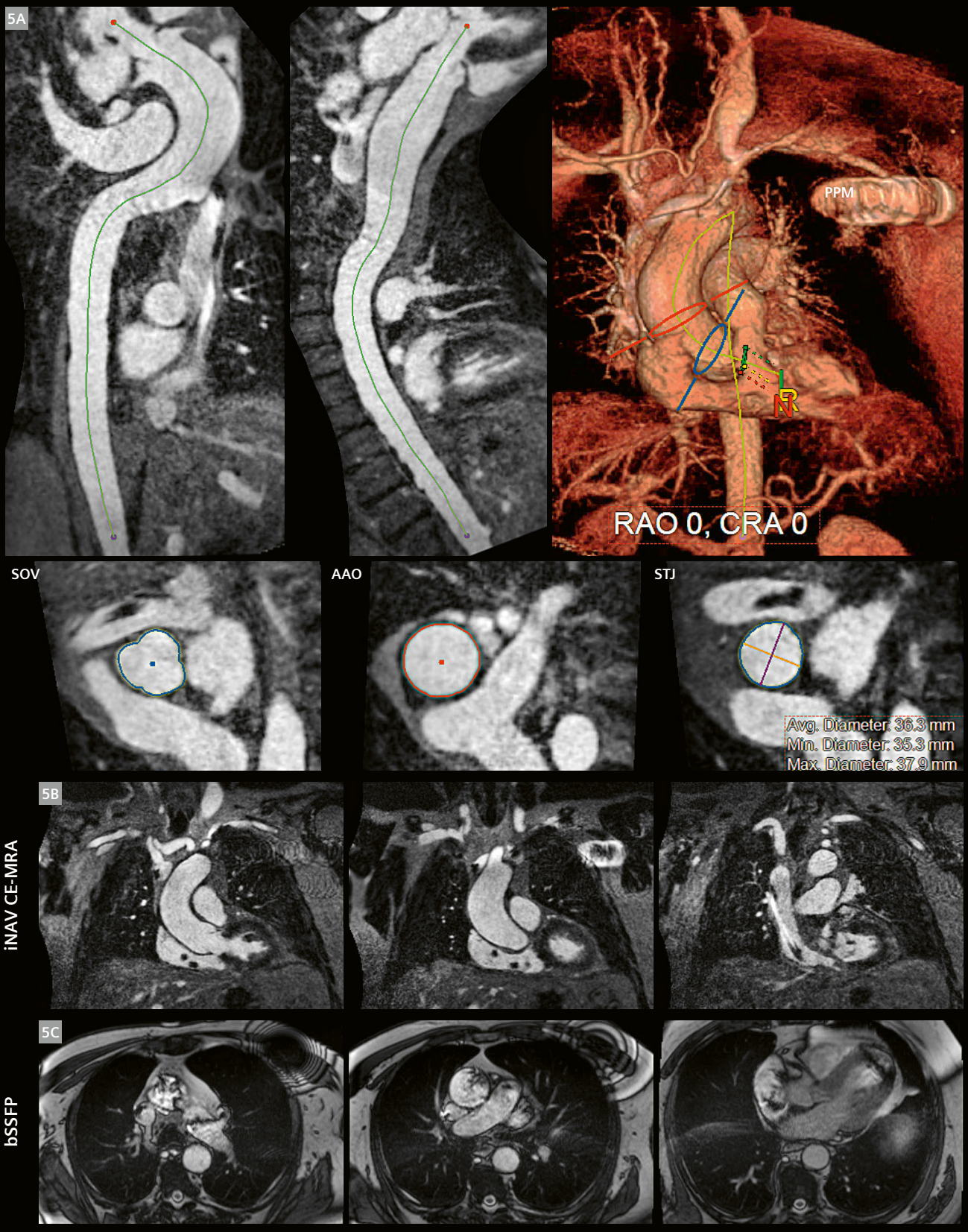

5 **(5A)** iNAV CE-MRA without wideband inversion recovery. Centerline semiautomated aortic measurements (CSAM) in a patient with permanent cardiac pacemaker. **(5B)** iNAV CE-MRA is free from significant artifact in the pertinent anatomical structures compared to balanced steady-state free precession (bSSFP) **(5C).**

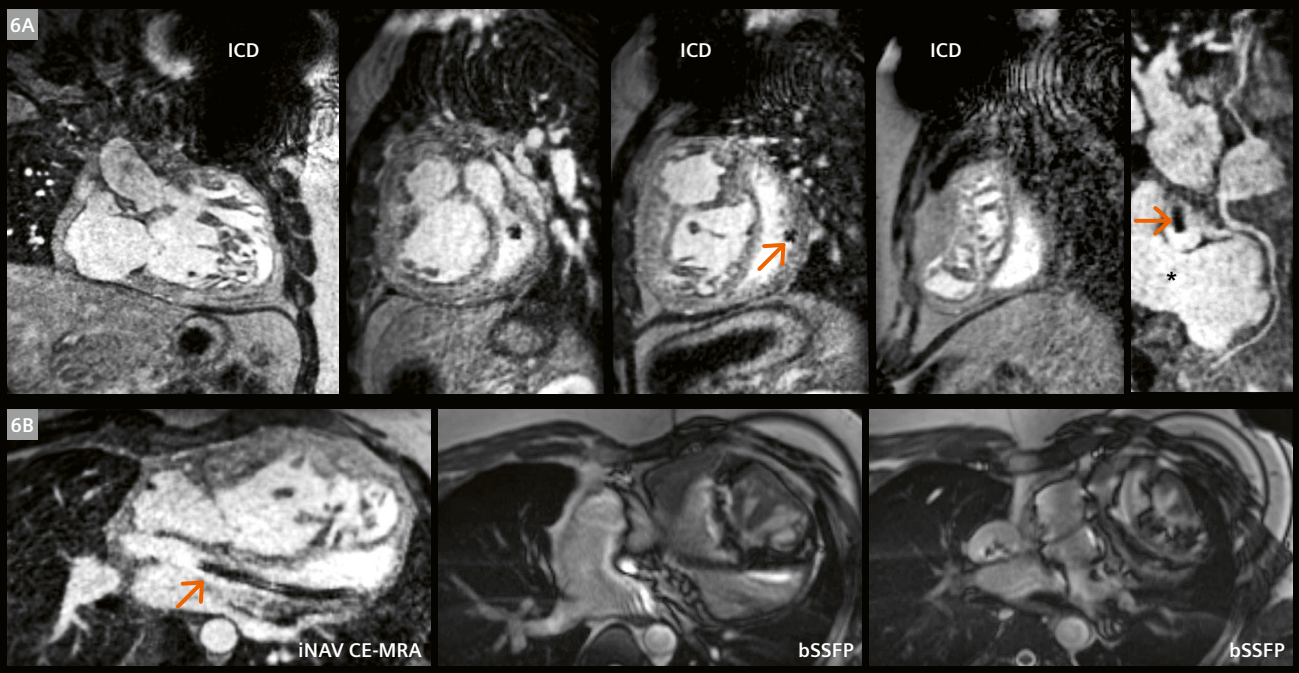

6 A 46-year-old male with a history of D-transposition of the great arteries, status post-atrial switch procedure. Systemic outflow tract **(6A)** and short-axis views demonstrate enlargement of the systemic ventricle and large signal void artifact from the internal cardiac defibrillator (ICD). The coronary artery origins are normal, with demonstration of systemic venous baffle patency and ICD lead within (orange arrows). The pulmonary venous baffle (asterisk) is also widely patent. Extensive artifact is present on balanced steady-state free precession (bSSFP) images compared to wideband iNAV CE-MRA **(6B)**.

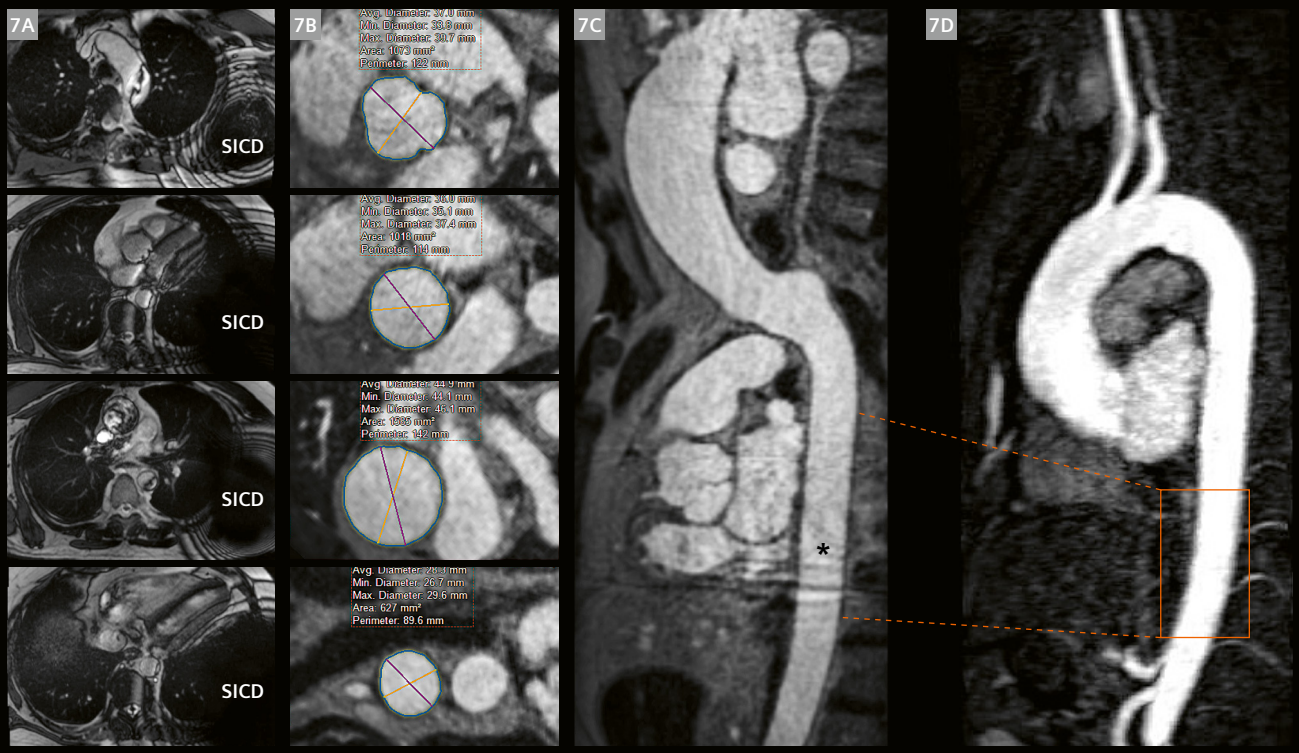

7 A 59-year-old male with subcutaneous internal cardiac defibrillator (SICD). **(7A)** Balanced steady-state free precession (bSSFP) axial images contain extensive artifacts. **(7B)** Centerline semiautomated aortic measurements (CSAM) of the sinus of Valsalva, sinotubular junction, ascending aorta, and arch are still feasible. **(7C)** With use of wideband iNAV CE-MRA, rippling artifacts (asterisks) were still present, overlaying the thoracic descending aorta; however, **(7D)** time-resolved MRA is free from artifacts.

Full aortic imaging

Lifelong aortic surveillance is needed after surgical repair or for medically treated disease. Full-field-of-view coronal imaging is not adequate to capture the entire aorta, arch vessels, and iliofemoral vessels in all patients. Therefore, a combination of acquisitions is often necessary.

Several non-contrast techniques have been used for abdominopelvic MRA. IR inflow techniques are most suitable for small-volume acquisitions. Quiescent-interval single-shot (QISS), with bSSFP, or radial FLASH readout can be acquired with breath-hold or free breathing, respectively, although the former is susceptible to inhomogeneity artifacts. Furthermore, all the above techniques require cardiac gating, which reduces acquisition efficiency. More recent developments include ungated 3D T2-prepared Dixon GRE. However, navigator gating and a comparatively longer repetition time likewise decrease the efficiency of the technique. While large-volume non-contrast techniques require an acquisition duration that spans several minutes, first-pass CE-MRA can be performed in a single breath-hold.

First-pass CE-MRA can be readily combined with iNAV CE-MRA with or without TWIST (Figs. 3, 4, 8, and 9) to provide extended coverage since aortic dissection and manifestations of systemic illnesses may not be isolated to the thoracic region (Fig. 10). Without TWIST, arterial and venous phase high-resolution abdominopelvic CE-MRA images are acquired with Care Bolus, immediately followed by iNAV CE-MRA. Without injector pause, the 0.1 mmol/kg GBCA continuous infusion is administered after the initial contrast/saline bolus combination. Because first-pass MRA is acquired with 0.1 mmol/kg of GBCA, (instead of the standard TWIST dose of 0.05 mmol/kg), the extra intravascular signal is used to acquire iNAV CE-MRA at 1.2 mm isotropic spatial resolution with higher acceleration factor and no overall increase in acquisition duration. Figure 9 is an example of full aortic imaging acquired using first-pass abdominopelvic MRA followed by iNAV CE-MRA at 1.2 mm isotropic spatial resolution.

For TEVAR hybrid repairs, TWIST is important for evaluation of the endograft. For this protocol, we start with the standard TWIST using 0.05 mmol/kg of 1-molar contrast agent with 30 mL saline, followed by 0.1 mmol/kg GBCA infusion for iNAV CE-MRA without delay. This is followed by Care Bolus and first-pass CE-MRA of the abdomen and pelvis with the remaining 0.05 mmol/kg GBCA.

Combined iNAV CE-MRA and LGE imaging

Many conditions, such as hypertension, vasculitis, and atherosclerotic disease, affect the thoracic vasculature and have downstream effects on the myocardium. Depending on the indication or clinical question, both thoracic MRA and cardiac MRI may be required within the same exam (Fig. 11). Tissue characterization with delayed enhancement imaging and extracellular volume fraction provide highly desirable information; therefore, it may be preferable to acquire gated MRA using GBCA. iNAV CE-MRA is compatible with the typical workhorses of the CMR imaging suite, such as bSSFP cine, post-contrast T1 parametric mapping, and late gadolinium enhancement.

Assessing intracardiac anatomy

4D flow has proven effective in quantifying hemodynamic properties across a large volume of anatomical coverage, given the ability to retrospectively prescribe any slice plane for analysis. Characterization of relatively low intracardiac velocities is most impacted by limited velocity-to-noise ratio (VNR) without GBCA at 1.5T. Technical adjustments may be required to increase acquired voxel size and to lower the acceleration factor and/or the receiver bandwidth as compensation. The proposition of highly undersampled *k*-space acquisition with Compressed-Sensing reconstruction is especially attractive, given the significantly shorter acquisition time. Compared to conventional 4D flow, there is significant underestimation of mitral-valve forward and net volumes, early-to-active left ventricular filling velocity ratio [17], aortic-valve forward volume, peak aortic systolic velocity [18], and higher noise values with increasing acceleration factors [19]. As a contrast-enhanced technique, iNAV CE-MRA provides the secondary benefit of boosting 4D flow SNR by up to 1.8× [19], which can be traded for higher spatiotemporal fidelity. Additionally, a key advantage of gated iNAV CE-MRA is the assessment of intracardiac structure and anatomical defects. These include atrial and ventricular septal defects, and arteriovenous connections. The high-resolution anatomic information is complementary to phase-contrast MRI quantitative flow data (Fig. 12).

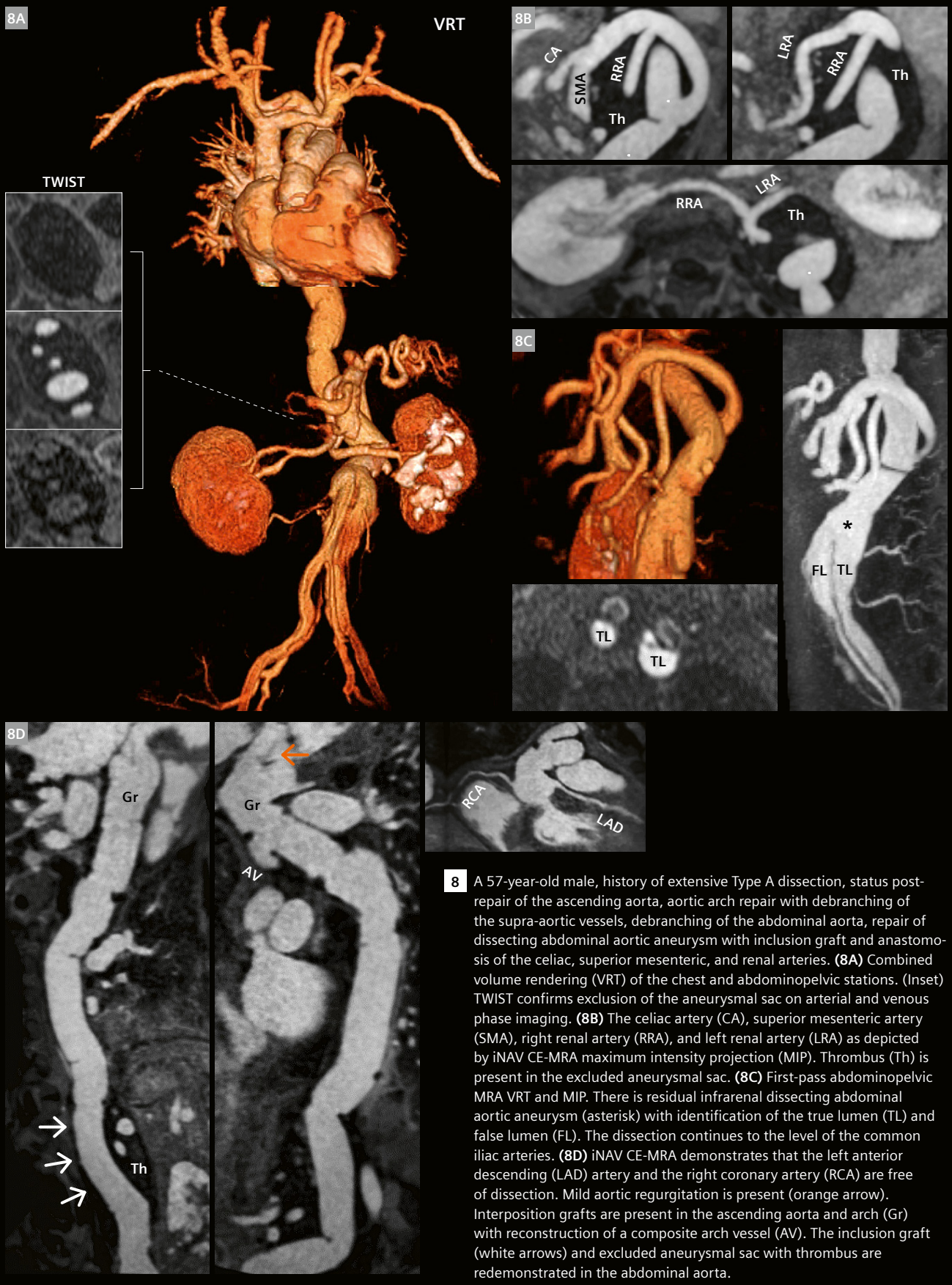

8 A 57-year-old male, history of extensive Type A dissection, status post-repair of the ascending aorta, aortic arch repair with debranching of the supra-aortic vessels, debranching of the abdominal aorta, repair of dissecting abdominal aortic aneurysm with inclusion graft and anastomosis of the celiac, superior mesenteric, and renal arteries. **(8A)** Combined volume rendering (VRT) of the chest and abdominopelvic stations. (Inset) TWIST confirms exclusion of the aneurysmal sac on arterial and venous phase imaging. **(8B)** The celiac artery (CA), superior mesenteric artery (SMA), right renal artery (RRA), and left renal artery (LRA) as depicted by iNAV CE-MRA maximum intensity projection (MIP). Thrombus (Th) is present in the excluded aneurysmal sac. **(8C)** First-pass abdominopelvic MRA VRT and MIP. There is residual infrarenal dissecting abdominal aortic aneurysm (asterisk) with identification of the true lumen (TL) and false lumen (FL). The dissection continues to the level of the common iliac arteries. **(8D)** iNAV CE-MRA demonstrates that the left anterior descending (LAD) artery and the right coronary artery (RCA) are free of dissection. Mild aortic regurgitation is present (orange arrow). Interposition grafts are present in the ascending aorta and arch (Gr) with reconstruction of a composite arch vessel (AV). The inclusion graft (white arrows) and excluded aneurysmal sac with thrombus are redemonstrated in the abdominal aorta.

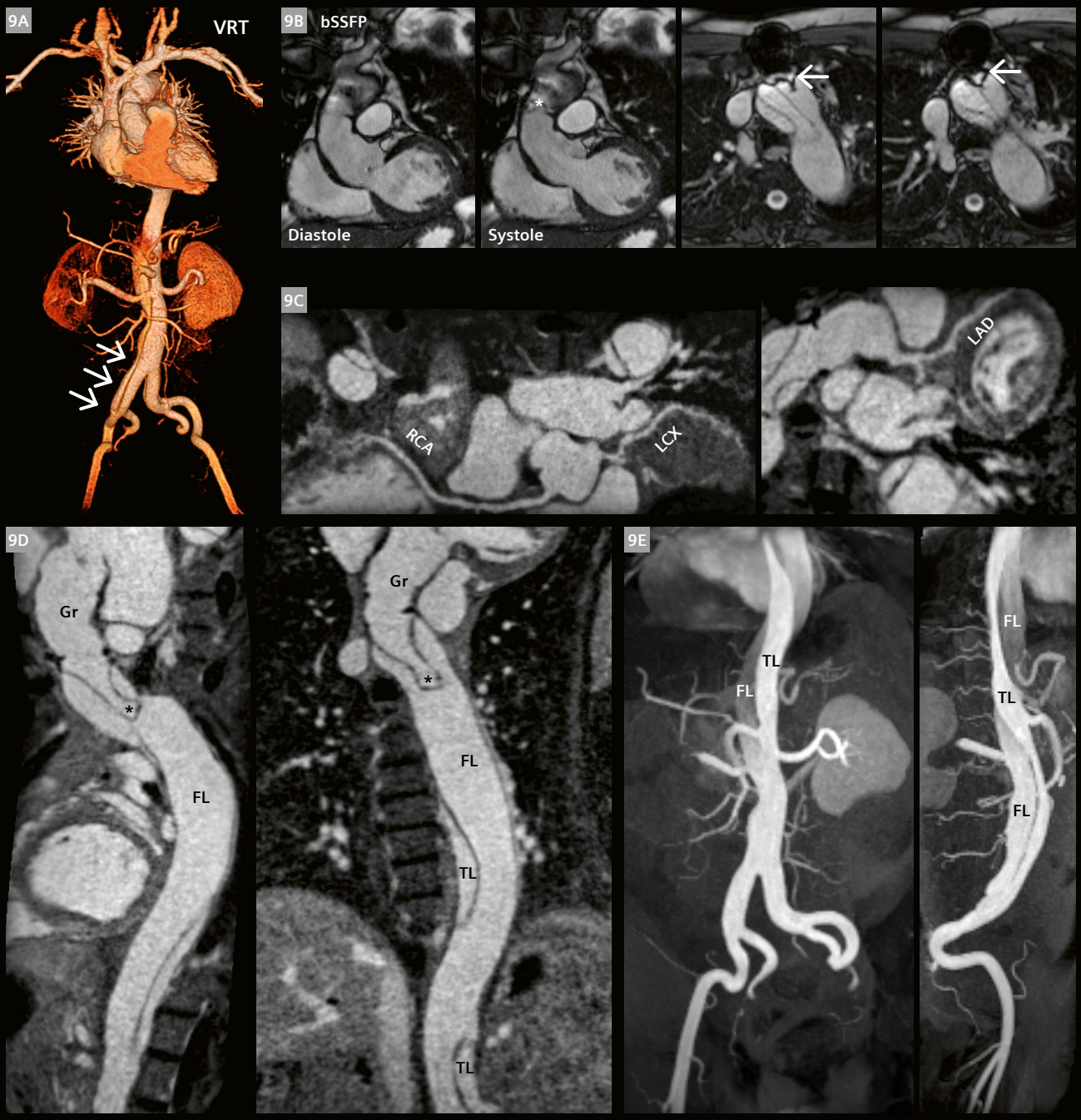

9 A 58-year-old male with a history of Type A aortic dissection, status post-repair. Whole-chest acquisition duration was 4.84 minutes with 1.2 mm isotropic acquired spatial resolution. **(9A)** Volume rendering (VRT) of the combined iNAV and first-pass CE-MRA with coverage to the level of the femoral vessels. Residual aortic dissection extending to the right common iliac artery and infrarenal aortic aneurysm is visible (white arrows). **(9B)** Complex to-and-fro flow patterns across the dissection flap (white asterisk) result in dephasing artifacts on balanced steady-state free precession (bSSFP) images. Susceptibility artifacts from sternal wires also encroach into the aortic arch intravascular space (white arrows). **(9C)** The right coronary artery (RCA), left anterior descending (LAD) artery, and left circumflex (LCX) artery are free from dissection. **(9D)** In comparison to bSSFP, iNAV CE-MRA curved multiplanar reconstructions (MPRs) are free from significant artifacts. Distal to the ascending aortic graft (Gr) insertion, the dissection flap (black asterisk), false lumen (FL), and true lumen (TL) can be visualized. **(9E)** Maximal intensity projection (MIP) of first-pass abdominopelvic MRA demonstrates continuation of aortic dissection of true lumen (TL) and false lumen (FL) to the abdominal aorta.

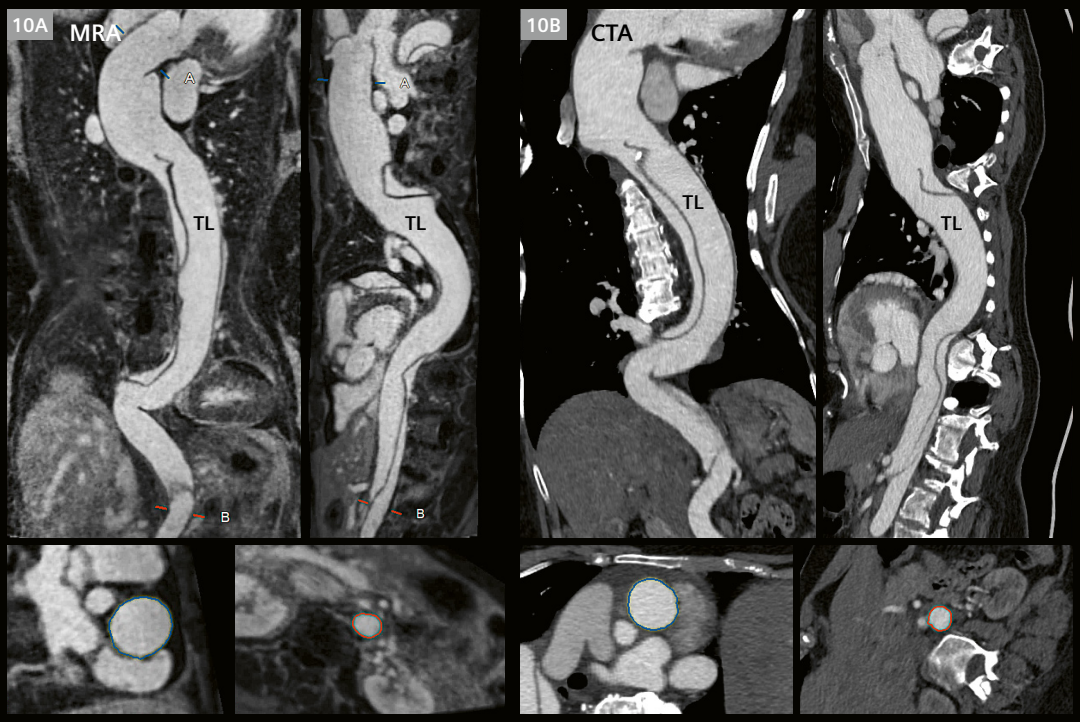

10 Comparison of iNAV CE-MRA **(10A)** and CTA **(10B)** curved multiplanar reconstruction (MPR) images in a patient with Type A aortic dissection extending beyond the thoracic station.

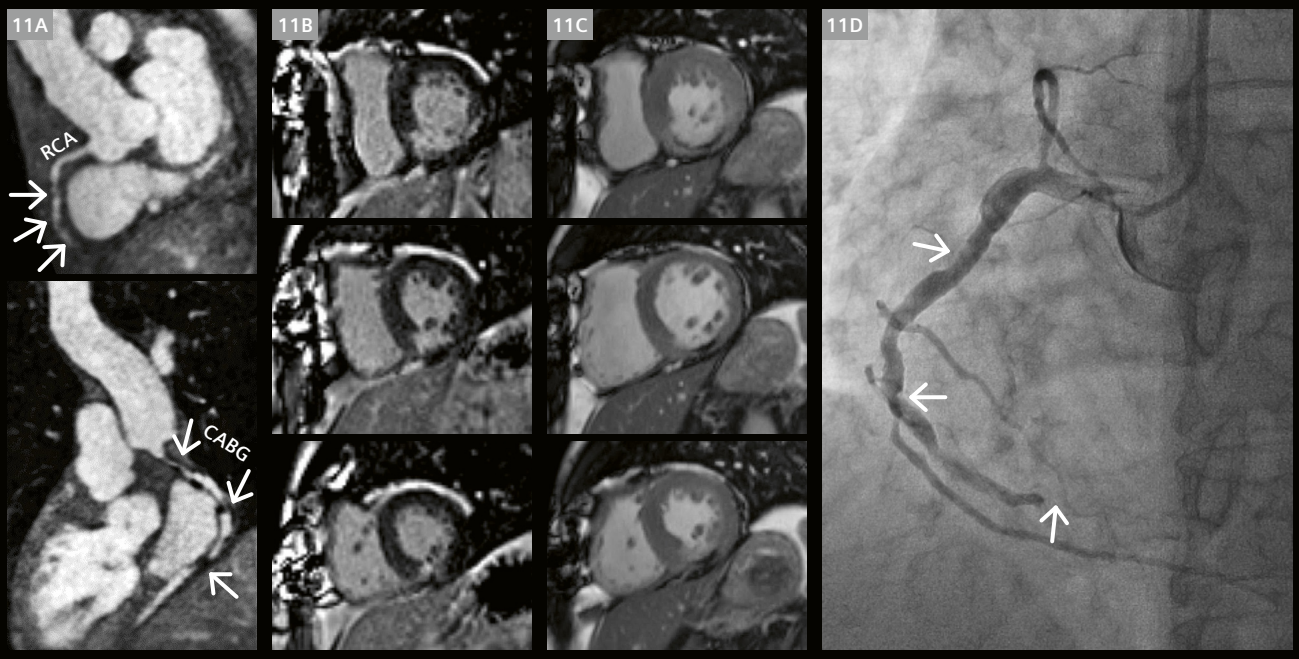

11 A 62-year-old male with a history of coronary artery disease and coronary artery bypass grafts. **(11A)** Multifocal stenosis and midvessel occlusion (white arrows) are present in the right coronary artery (RCA), with severe disease of the coronary artery bypass graft (CABG) to posterior descending artery (white arrows). **(11B, 11C)** Late gadolinium enhancement and cine images respectively demonstrate inferior wall myocardial infarction. **(11D)** Invasive coronary angiogram in the same patient with corresponding stenosis and occlusion of the mid-RCA (white arrows).

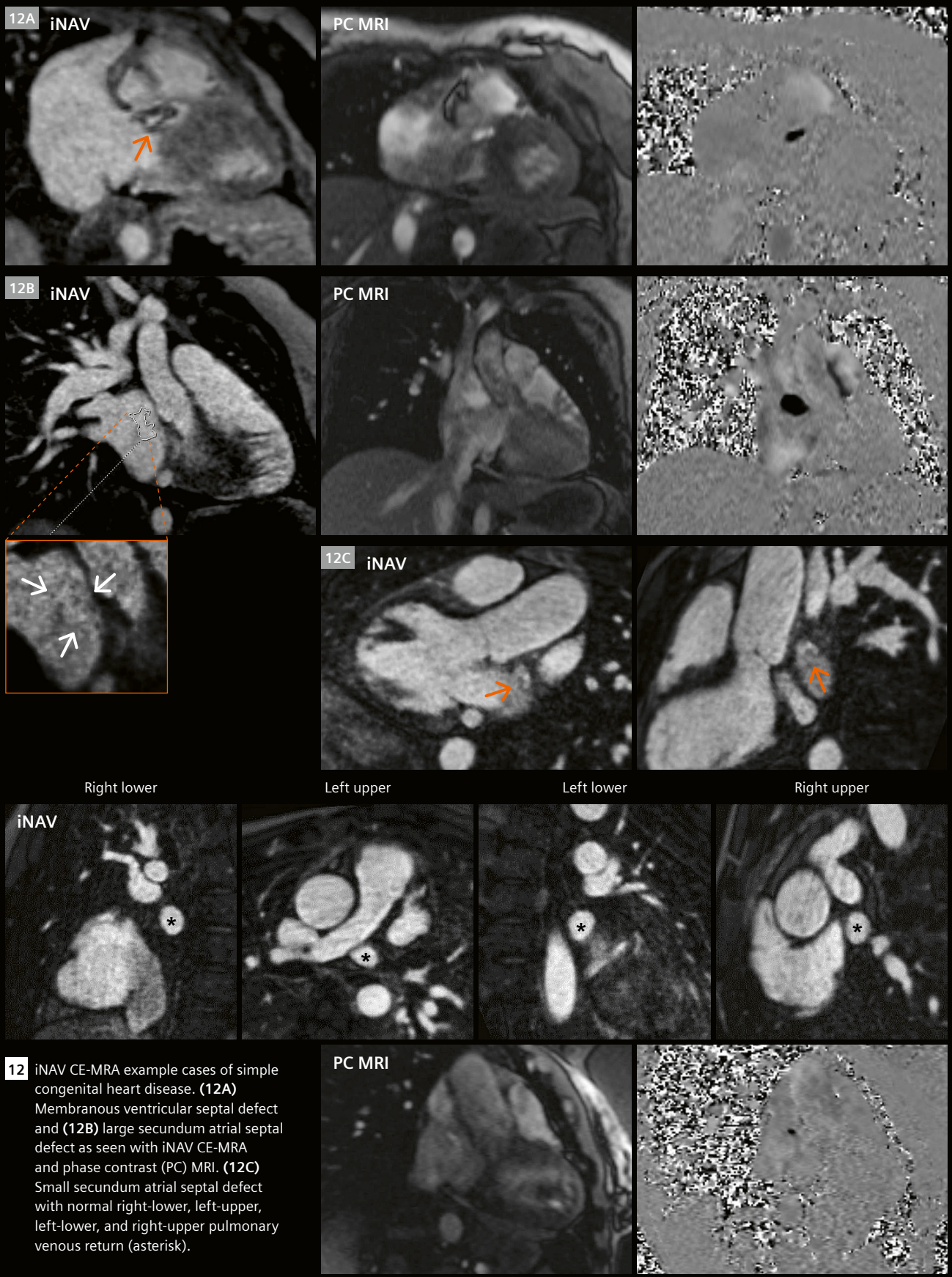

12 iNAV CE-MRA example cases of simple congenital heart disease. **(12A)** Membranous ventricular septal defect and **(12B)** large secundum atrial septal defect as seen with iNAV CE-MRA and phase contrast (PC) MRI. **(12C)** Small secundum atrial septal defect with normal right-lower, left-upper, left-lower, and right-upper pulmonary venous return (asterisk).

In summary, with the iNAV/VD-CASPR framework gated MRA can be performed with 100% respiratory efficiency and thus with a predictable acquisition duration. Both non-contrast and contrast-enhanced techniques have been used, each with its own distinct advantages and disadvantages. iNAV CE-MRA can be combined with TWIST and abdominopelvic first-pass CE-MRA for dynamic information and/or extended coverage, respectively. Based on our single-center experience, this allows for versatile and efficient imaging that shows promise in complex patients with extensive aortic repairs, obesity, and implantable cardiac devices and is robust to magnetic field inhomogeneity and local susceptibility artifacts.

References

1 Munoz C, Bustin A, Neji R, Kunze KP, Forman C, Schmidt M, et al. Motion-corrected 3D whole-heart water-fat high-resolution late gadolinium enhancement cardiovascular magnetic resonance imaging. J Cardiovasc Magn Reson. 2020;22(1):53.

2 Groarke JD, Waller AH, Vita TS, Michaud GF, Di Carli MF, Blankstein R, et al. Feasibility study of electrocardiographic and respiratory gated, gadolinium enhanced magnetic resonance angiography of pulmonary veins and the impact of heart rate and rhythm on study quality. J Cardiovasc Magn Reson. 2014;16(1):43.

3 Siebermair J, Kholmovski EG, Sheffer D, Schroeder J, Jensen L, Kheirkhahan M, et al. Saturation recovery-prepared magnetic resonance angiography for assessment of left atrial and esophageal anatomy. Br J Radiol. 2021;94(1123):20210048.

4 Craft J, Parikh R, Cheng JY, Diaz N, Kunze KP, Schmidt M, et al. Isotropic, high-resolution, whole-chest inversion recovery contrast-enhanced magnetic resonance angiography in under 4.5 min using image-based navigator fluoro trigger. Front Cardiovasc Med. 2025;12:1549275.

5 Bley TA, Wieben O, François CJ, Brittain JH, Reeder SB. Fat and water magnetic resonance imaging. J Magn Reson Imaging. 2010;31(1):4–18.

6 Wood G, Pedersen AU, Kunze KP, Neji R, Hajhosseiny R, Wetzl J, et al. Automated detection of cardiac rest period for trigger delay calculation for image-based navigator coronary magnetic resonance angiography. J Cardiovasc Magn Reson. 2023;25(1):52.

7 NCD Risk Factor Collaboration (NCD-RisC). Worldwide trends in underweight and obesity from 1990 to 2022: a pooled analysis of 3663 population-representative studies with 222 million children, adolescents, and adults. Lancet. 2024;403(10431):1027–1050.

8 Thorpe KE, Joski PJ. Estimated Reduction in Health Care Spending Associated With Weight Loss in Adults. JAMA Netw Open. 2024;7(12):e2449200.

9 Tandon A, Hashemi S, Parks WJ, Kelleman MS, Sallee D, Slesnick TC. Improved high-resolution pediatric vascular cardiovascular magnetic resonance with gadofosveset-enhanced 3D respiratory navigated, inversion recovery prepared gradient echo readout imaging compared to 3D balanced steady-state free precession readout imaging. J Cardiovasc Magn Reson. 2016;18(1):74.

10 Craft J, Weber J, Li Y, Cheng JY, Diaz N, Kunze KP, et al. Inversion recovery and saturation recovery pulmonary vein MR angiography using an image based navigator fluoro trigger and variable-density 3D cartesian sampling with spiral-like order. Int J Cardiovasc Imaging. 2024;40(6):1363–1376.

11 Sperry BW, Vamenta MS, Gunta SP, Thompson RC, Einstein AJ, Castillo M, et al. Influence of Body Mass Index on Radiation Exposure Across Imaging Modalities in the Evaluation of Chest Pain. J Am Heart Assoc. 2024;13(8):e033566.

12 Mazzolai L, Teixido-Tura G, Lanzi S, Boc V, Bossone E, Brodmann M, et al. 2024 ESC Guidelines for the management of peripheral arterial and aortic diseases. Eur Heart J. 2024;45(36):3538–3700.

13 Habets J, Zandvoort HJ, Reitsma JB, Bartels LW, Moll FL, Leiner T, et al. Magnetic resonance imaging is more sensitive than computed tomography angiography for the detection of endoleaks after endovascular abdominal aortic aneurysm repair: a systematic review. Eur J Vasc Endovasc Surg. 2013;45(4):340–50.

14 Ammannaya GKK. Implantable cardioverter defibrillators – the past, present and future. Arch Med Sci Atheroscler Dis. 2020;5:e163–e170.

15 Bhatia N, El-Chami M. Leadless pacemakers: a contemporary review. J Geriatr Cardiol. 2018;15(4):249–253.

16 Ibrahim EH, Runge M, Stojanovska J, Agarwal P, Ghadimi-Mahani M, Attili A, et al. Optimized cardiac magnetic resonance imaging inversion recovery sequence for metal artifact reduction and accurate myocardial scar assessment in patients with cardiac implantable electronic devices. World J Radiol. 2018;10(9):100–107.

17 Varga-Szemes A, Halfmann M, Schoepf UJ, Jin N, Kilburg A, Dargis DM, et al. Highly Accelerated Compressed-Sensing 4D Flow for Intracardiac Flow Assessment. J Magn Reson Imaging. 2023;58(2):496–507.

18 Neuhaus E, Weiss K, Bastkowski R, Koopmann J, Maintz D, Giese D. Accelerated aortic 4D flow cardiovascular magnetic resonance using compressed sensing: applicability, validation and clinical integration. J Cardiovasc Magn Reson. 2019;21(1):65.

19 Hess AT, Bissell MM, Ntusi NA, Lewis AJ, Tunnicliffe EM, Greiser A, et al. Aortic 4D flow: quantification of signal-to-noise ratio as a function of field strength and contrast enhancement for 1.5T, 3T, and 7T. Magn Reson Med. 2015;73(5):1864–71.

Contact

Jason Craft, M.D.
Director, Cardiac MRI
Good Samarian University Hospital
West Islip, NY, USA

Associate Director, Cardiac MRI
St Francis Hospital & Heart Center
100 Port Washington Blvd
Roslyn, NY 11576
USA
Jason.craft@chsli.org